AMERICAN SOCIETY FOR MICROBIOLOGY | mBio®

RESEARCH ARTICLE

Morphological and Transcriptional Responses to CRISPRi Knockdown of Essential Genes in *Escherichia coli*

Melanie R. Silvis,[a] Manohary Rajendram,[b] Handuo Shi,[c] Hendrik Osadnik,[a] Andrew N. Gray,[a] Spencer Cesar,[c] Jason M. Peters,[d] Cameron C. Hearne,[a] Parth Kumar,[a] Horia Todor,[a] Kerwyn Casey Huang,[b,c,e] Carol A. Gross[a]

[a]Department of Cell and Tissue Biology, University of California San Francisco, San Francisco, California, USA
[b]Department of Bioengineering, Stanford University, Stanford, California, USA
[c]Department of Microbiology and Immunology, Stanford University School of Medicine, Stanford, California, USA
[d]Pharmaceutical Sciences Division, School of Pharmacy, University of Wisconsin—Madison, Madison, Wisconsin, USA
[e]Chan Zuckerberg Biohub, San Francisco, California, USA

Melanie R. Silvis, Manohary Rajendram, Handuo Shi, and Hendrik Osadnik contributed equally to this work. Author order was determined by mutual agreement.

ABSTRACT CRISPR interference (CRISPRi) has facilitated the study of essential genes in diverse organisms using both high-throughput and targeted approaches. Despite the promise of this technique, no comprehensive arrayed CRISPRi library targeting essential genes exists for the model bacterium *Escherichia coli*, or for any Gram-negative species. Here, we built and characterized such a library. Each of the ~500 strains in our *E. coli* library contains an inducible, chromosomally integrated single guide RNA (sgRNA) targeting an essential (or selected nonessential) gene and can be mated with a pseudo-Hfr donor strain carrying a *dcas9* cassette to create a CRISPRi knockdown strain. Using this system, we built an arrayed library of CRISPRi strains and performed population and single-cell growth and morphology measurements as well as targeted follow-up experiments. These studies found that inhibiting translation causes an extended lag phase, identified new modulators of cell morphology, and revealed that the morphogene *mreB* is subject to transcriptional feedback regulation, which is critical for the maintenance of morphology. Our findings highlight canonical and noncanonical roles for essential genes in numerous aspects of cellular homeostasis.

IMPORTANCE Essential genes make up only ~5 to 10% of the genetic complement in most organisms but occupy much of their protein synthesis and account for almost all antibiotic targets. Despite the importance of essential genes, their intractability has, until recently, hampered efforts to study them. CRISPRi has facilitated the study of essential genes by allowing inducible and titratable depletion. However, all large-scale CRISPRi studies in Gram-negative bacteria thus far have used plasmids to express CRISPRi components and have been constructed in pools, limiting their utility for targeted assays and complicating the determination of antibiotic effects. Here, we use a modular method to construct an arrayed library of chromosomally integrated CRISPRi strains targeting the essential genes of the model bacterium *Escherichia coli*. This library enables targeted studies of essential gene depletions and high-throughput determination of antibiotic targets and facilitates studies targeting the outer membrane, an essential component that serves as the major barrier to antibiotics.

KEYWORDS arrayed library, CRISPRi, *Escherichia coli*, essential genes, microscopy

Reverse genetic approaches based on gene inactivation have been responsible for elucidating the function of many bacterial genes (1–4). Essential genes, which encode the key reactions of life and represent a large fraction of a cell's protein budget

Citation Silvis MR, Rajendram M, Shi H, Osadnik H, Gray AN, Cesar S, Peters JM, Hearne CC, Kumar P, Todor H, Huang KC, Gross CA. 2021. Morphological and transcriptional responses to CRISPRi knockdown of essential genes in *Escherichia coli*. mBio 12:e02561-21. https://doi.org/10.1128/mBio.02561-21.

Editor Susan Gottesman, National Cancer Institute

Address correspondence to Horia Todor, horia.todor@gmail.com, Kerwyn Casey Huang, kchuang@stanford.edu, or Carol A. Gross, cgrossucsf@gmail.com.

This article is a direct contribution from Carol A. Gross, a Fellow of the American Academy of Microbiology, who arranged for and secured reviews by Jan-Willem Veening, University of Lausanne; Thomas Bernhardt, Harvard Medical School; and David Bikard, Institut Pasteur.

Received 2 September 2021
Accepted 9 September 2021
Published 12 October 2021

(5), are not amenable to such approaches because, by definition, their deletion renders cells inviable. CRISPR interference (CRISPRi) provides inducible knockdown of bacterial gene expression (6, 7) and has enabled genetic approaches to studying essential gene function. Arrayed libraries of CRISPRi strains targeting essential genes have been of particular utility, because they enable flexible pooling and candidate follow-ups of pooled assays as well as single-strain assays such as microscopy. Such libraries have been described for *Bacillus subtilis* (8), *Streptococcus pneumoniae* (9), *Streptococcus mutans* (10), and *Mycobacterium smegmatis* (11) and have been used to yield surprising cross-pathway functional interactions, insights into cellular vulnerabilities, and functional characterizations of essential genes. Remarkably, no such library has been described for any Gram-negative bacterium despite the original demonstration of CRISPRi in *Escherichia coli* (7), the veritable cornucopia of pooled CRISPRi studies in Gram-negative bacteria (reviewed in reference 12), and the significant differences between Gram-negative and Gram-positive physiology centered around essential functions such as the Gram-negative-specific outer membrane.

Here, we describe the design and construction of such a library in *E. coli*. Motivated by the potential to uncover both fundamental and clinically relevant principles governing bacterial growth, we profiled the morphological and growth phenotypes of our library. We discovered increased lag upon knockdown of ribosomal genes, novel modulators of cell morphology, and a critical transcriptional feedback circuit affecting the expression of the cell shape gene *mreB*. This library, which is available from the Coli Genetic Stock Center, will be a resource for the microbiology community and will contribute to a deeper understanding of Gram-negative bacteria.

RESULTS

A partial arrayed library of chromosomally encoded CRISPRi strains. Previous CRISPRi systems in *E. coli* (7, 13–18) used plasmids to express the single guide RNA (sgRNA) component of the CRISPRi system and were constructed and screened in pools. Although such libraries enable quantification of growth phenotypes, they are unsuitable for targeted assays such as single-strain profiling of morphology and growth dynamics, and the need to grow them under selection may complicate the determination of phenotypes such antibiotic sensitivities. To overcome these limitations, we constructed an arrayed library containing a chromosomally encoded CRISPRi system targeting the essential genes of *E. coli* (see Materials and Methods; also, see Table S1 in the supplemental material). Briefly, sgRNAs targeting the 5′ ends of all essential open reading frames (ORFs) and selected nonessential genes (Table S1) were integrated at the lambda *att* site of *E. coli* BW25113 under the control of an IPTG (isopropyl-β-D-thiogalactopyranoside)-inducible promoter (see Materials and Methods) as previously described (19). CRISPRi strains were constructed using a high-efficiency conjugation system to transfer *dcas9* from the chromosome of a pseudo-Hfr donor strain to the chromosomal Tn*7* *att* site of the sgRNA-encoding recipient (Fig. 1A; Materials and Methods). We quantified the performance of our system by measuring its ability to repress *rfp* expression. Our CRISPRi system achieved ~50% knockdown of *rfp* in the absence of inducer (due to basal expression of the sgRNA) and uniform, concentration-dependent knockdown of *rfp* upon sgRNA induction with IPTG (Fig. 1B; Materials and Methods).

The construction of our library (see Materials and Methods) differed from that of other arrayed libraries (8–11) in that sgRNAs were cloned, integrated, single-colony purified, and sequence verified (Fig. S1A; Table S1) prior to the introduction of *dcas9*. While this method limits the rise of suppressors during strain construction, errors during the additional handling required to introduce *dcas9* into the sgRNA strains unfortunately led to substantial cross-contamination of the CRISPRi strains. This cross-contamination affected ~30% of our CRISPRi strains (contamination fraction of $>10^{-4}$ based on deep sequencing of each strain) (Table S1; Fig. S1B) but not the sgRNA strains (Table S1; Fig. S1A). Unfortunately, the cross-contamination was not discovered until

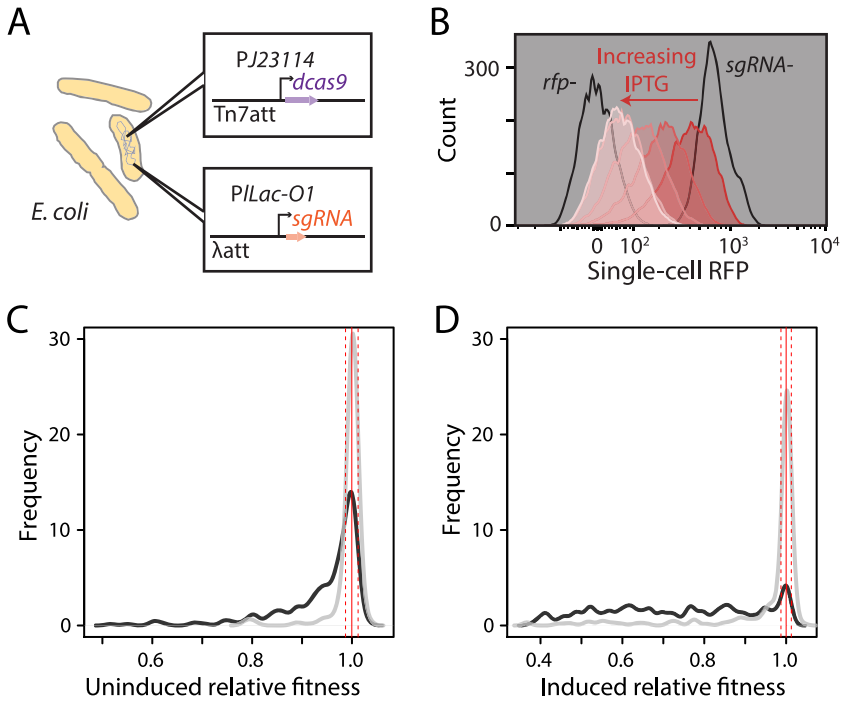

FIG 1 CRISPRi induction reduces fitness when targeting essential genes. (A) Schematic of the *E. coli* CRISPRi system showing the integration sites and promoters of the *sgRNA* and *dcas9* constructs. (B) CRISPRi targeting *rfp* expression achieved titratable and unimodal knockdown at various IPTG levels. The red histograms correspond to 0, 0.03125, 0.0625, 0.125, and 1 mM IPTG. No RFP (*rfp*-) or full RFP expression (*sgRNA*-) is indicated in black. (C and D) Gaussian kernel density estimate of the distribution of relative fitness values for strains targeting essential (black) and nonessential (gray) genes with the CRISPRi system at basal induction (C) and full induction using 1 mM IPTG (D). The solid red line indicates the median of 48 nontargeting controls, and the dashed red lines indicate ±3 standard deviations (SD) from the median, estimated from the median absolute distance.

after data collection was completed. As such, we discuss only those results pertaining to the 372 uncontaminated CRISPRi strains (Table S1). These strains encompass all major essential processes (all Clusters of Orthologous Groups [COG], Gene Ontology [GO], and KEGG categories with more than 5 genes) and hence retain the potential to uncover systems-level physiological consequences of essential gene knockdown.

Pooled growth of the CRISPRi library illustrates essential gene dosage effects. To determine the effect of essential gene knockdown using our system, we constructed a pooled version of our library (see Materials and Methods) and quantified the relative fitness (RF; i.e., the number of doublings relative to that of nontargeted control strains) of each strain during pooled growth with and without induction of the CRISPRi system using next-generation sequencing. This approach was reproducible (Fig. S2), and because it uses the sgRNA sequence as a barcode, it was not affected by cross-contamination.

Slight (basal CRISPRi, no IPTG) knockdown of a majority of essential genes (54%; 152/282 strains) resulted in a significant fitness defect (>3 standard deviations [SD] below the nontargeting controls) (Fig. 1C). In contrast, slight knockdown of nonessential genes seldom caused a significant fitness defect (7%; 13/187 strains) (Fig. 1C). Despite the large fraction of essential-gene knockdown strains with a significant fitness defect, the magnitude of the effect was small (median RF_{ess} = 0.98) (Fig. 1C). Only 53 essential gene knockdown strains exhibited a fitness defect ≥10% (RF < 0.9), indicating that many essential gene products are present in excess in wild-type cells, likely to buffer against environmental fluctuations, as previously suggested by pooled and arrayed approaches in *E. coli*, *B. subtilis*, and other species (8, 10, 15, 18, 20).

Strong (fully induced CRISPRi, 1 mM IPTG) knockdown of most essential genes caused significant fitness defects relative to the nontargeting controls (80%; 225/282 strains), and these defects were substantial in magnitude (median RF_{ess} = 0.73) (Fig. 1D). In contrast,

knockdown of only a small fraction of nonessential genes (16%; 30/187 strains) caused reduced relative fitness even with induction (median $RF_{non\text{-}ess}$ = 1.00) (Fig. 1D), consistent with the general lack of growth phenotypes in most viable *E. coli* deletion strains in rich media without inhibitory chemicals (1, 2, 21).

Recent studies identified sequence determinants of sgRNA toxicity (22) and efficacy (23). However, we found that neither sgRNA toxicity (Fig. S3A and B) nor sgRNA activity (Fig. S3C to F) was significantly correlated with relative fitness in either the induced or uninduced condition, suggesting that these effects did not significantly affect the observed phenotypes. Taken together, these data highlight the nuanced growth effects of CRISPRi repression of essential genes and confirm that our system is specific and well calibrated to study the effects of both slight and strong essential-gene knockdown.

Growth consequences of slight knockdown of essential genes. Our pooled competitive growth assays identified a number of strains with significant fitness defects during growth with basal CRISPRi induction. However, these endpoint assays lacked the temporal resolution to determine whether decreased fitness is due to a lower maximal growth rate or a longer lag phase (see Materials and Methods). To determine the growth dynamics of our *E. coli* essential-gene knockdown strains with basal CRISPRi knockdown, we grew each of our strains overnight in LB, then diluted them into fresh medium, and measured their optical density (OD) in a plate reader as they resumed growth (Materials and Methods). Results were reproducible (Fig. S4A and B), and normalized maximal growth rates of individual strains were correlated with their fitness (RF) in the pooled screen ($r = 0.44$; $P < 2 \times 10^{-16}$) (Fig. 2A; Table S2), suggesting that most RF defects were due to slower growth rather than a longer lag phase.

Only 16 *E. coli* essential-gene knockdown strains exhibited significantly longer lag time (>3 SD higher than the median) (Fig. 2B; Table S2), a majority of which targeted ribosomal proteins (8/16 strains) and other translation-related genes (2/16 strains). The remainder targeted genes involved in cell division and DNA synthesis (*dnaA*, *ftsQ*, and *tmk*), and lipoprotein processing (*lolCD* and *lgt*). A previous study of the *E. coli* Keio knockout collection grown on agar plates identified long-lag phenotypes in strains with deletions of tRNA modification (e.g., *tusABCDE* and *rnt*) and ribosome maturation (e.g., *rimM*, *rbfA*, and *rgsA*) genes and hypothesized that a general decrease in translation efficiency may be responsible for this phenotype (24). Our observation that a majority (8/16 strains) of assayed essential ribosomal gene knockdown strains (*rps*, and *rpl*) exhibited long lag time strongly supports this hypothesis. Furthermore, when all essential ribosomal genes in our library were considered, lag time was correlated with the number of essential ribosomal genes in the targeted operon ($r = 0.71$; $P < 0.005$) (Fig. 2C). Strains targeting the largest ribosomal protein operons (the S10 and L14 operons) exhibited the longest lag times, potentially due to polar effects of CRISPRi knockdown (25) affecting the expression of multiple ribosomal proteins and thus amplifying the effect of these knockdowns on translational capacity.

To understand the manifestation of long lag times at the single-cell level, we selected three knockdown strains with long lag times, the *rpsS*, *dnaA*, and *ftsQ* strains, and imaged their emergence from stationary phase on agar pads while quantifying the instantaneous growth rates of individual cells. The instantaneous growth rate of individual cells was calculated as $1/V\ dV/dt$, which describes the relative rate of volume expansion, and is consistent with bulk measurements such as OD and CFU for steady-state cultures (26). During imaging, wild-type cells gradually increased their growth rate as they emerged from stationary phase until they reached ~0.03 min^{-1} (~23 min doubling time), usually after ~1.5 h (Fig. 2D). *ftsQ* knockdown cells similarly increased their growth rate, but for only ~60 min, after which growth rate plateaued and decreased (Fig. 2D). Decreased growth rate was associated with filamentation and some lysis (Fig. 2E). In contrast, many *dnaA* knockdown cells lysed by 1.5 h (Fig. 2E), and the cells that resumed growth exhibited low growth rates until ~2 h postdilution and reached maximum growth rates only after >3 h (Fig. S4C).

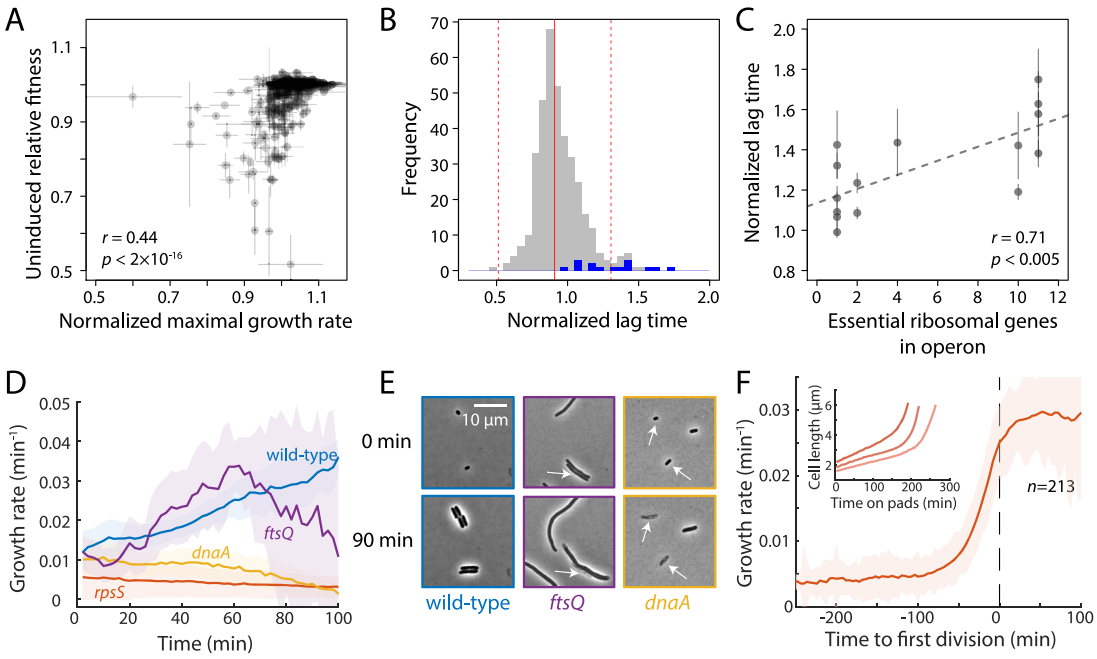

FIG 2 Strains with increased population-level lag time exhibit a range of single-cell phenotypes. (A) The maximum growth rate of strains grown individually without induction is correlated with their relative fitness in the pooled screen. Error bars represent the standard deviations (SD) for two biological replicates. (B) Histogram of lag times for CRISPRi strains normalized to WT. The solid red line indicates the median, and the dashed red lines indicate ±3 SD from the median, estimated from the median absolute distance. Blue bars denote ribosomal protein (*rps* and *rpl*) genes. (C) Normalized lag time is correlated with the number of essential ribosomal genes in the operon. The line denotes the linear best fit. (D) Single-cell instantaneous growth rates ($1/V\ dV/dt$) for three mutants with increased population-level lag times exhibited defects compared to wild-type after dilution of stationary-phase cells onto agarose pads with fresh medium. (E) The *ftsQ* and *dnaA* knockdown strains exhibited heterogeneity and growth defects during outgrowth from stationary phase. Most *ftsQ* knockdown cells first elongated, similar to the wild type, but later slowed growth (D) and failed to divide. A subset of *ftsQ* knockdown cells also lysed (white arrow). Many *dnaA* knockdown cells exhibited lysis (white arrows), and the remaining cells exhibited a lower growth rate than the wild-type (D), which increased only after 2 to 3 h (Fig. S4C). (F) *rpsS* cells increased growth rate concurrently with their first division after stationary-phase outgrowth. (Inset) Each *rpsS* cell first grew slowly and linearly for >100 min before transitioning into exponential-like growth. Data for three representative cells are shown. Data in panels D and F are means and SD.

The *rpsS* knockdown strain exhibited a previously uncharacterized behavior as it emerged from stationary phase: cells grew for several hours with slow, approximately linear kinetics (decreasing instantaneous growth rate with time) followed by a transition to exponential growth (Fig. 2F, inset). Interestingly, the transition to rapid growth tended to occur in a fixed window ~30 min prior to cell division (Fig. 2F), suggesting that cell division proceeds only after a reversal of slowdown. This long-lag phenotype persisted upon repeated regrowth and dilution, indicating that depletion of ribosomal proteins in stationary phase rather than genetic suppression of CRISPRi activity likely underlies this phenomenon. These results highlight the variability of single-cell phenotypes that can underlie slow growth caused by slight knockdown of essential genes and demonstrate a requirement for translational capacity during the transition from stationary to exponential growth. It is likely that a comprehensive analysis of single-cell growth rates and morphologies will identify both additional genes and phenotypes.

Morphological profiling identifies genes required for normal cell shape. Decreased growth rate is just one reflection of altered cellular homeostasis caused by the knockdown of essential genes. To more broadly determine how partial knockdown affects cellular physiology, we quantified the cellular dimensions of all strains in our library in the presence of basal CRISPRi knockdown after 3.5 h of growth in fresh LB. After correcting for plate effects (see Materials and Methods), most strains exhibited wild-type length and width (90%; 310/346 strains) (Fig. 3A; Table S3). A total of 23 strains were significantly wider than the median (>3 SD wider than the median) and 25 strains

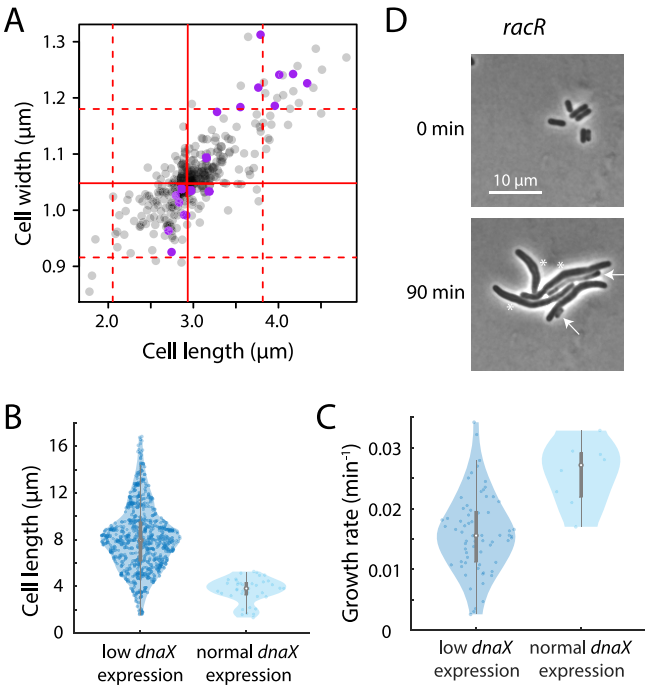

FIG 3 Heterogeneity in cell length can be linked to expression level or growth defects. (A) Cell length and width corrected for plate effects (Materials and Methods) of all strains in the uninduced condition. Solid red lines indicate the median width and length, and the dashed red lines indicate ±3 standard deviations (SD) from the median, estimated from the median absolute distance. Purple dots are outer membrane-related genes. (B and C) During outgrowth from stationary phase, *dnaX* cells exhibited heterogeneity in *dnaX* expression. Cells with low *dnaX* expression filamented (B) and grew more slowly (C) than cells with higher *dnaX* expression. (D) The *racR* strain exhibited filamentation, bulging (white asterisks), and lysis (white arrows) during outgrowth.

were significantly longer (Table S3). A majority of strains with altered dimensions (55%; 17/31 strains) were both significantly longer and significantly wider (Fig. 3A), suggesting a general breakdown of morphological homeostasis in these strains.

As reported in previous studies (21), we found that length heterogeneity within a strain (quantified by the coefficient of variation [CV]) was much greater than width variability (Table S3). To better understand sources of length variability, we performed time-lapse imaging of two strains with high length variability in which a monocistronic operon was targeted (*racR* and *dnaX*). Imaging of the *dnaX* (DNA polymerase III τ subunit) knockdown strain revealed bimodality in both growth rate and cell length. This heterogeneity likely reflects noise in *dnaX* knockdown levels, as imaging of *dnaX* cells containing a green fluorescent protein (GFP) reporter of *dnaX* expression (27) revealed that low-expression cells were longer (Fig. 3B) and grew more slowly than high-expression cells (Fig. 3C). The *racR* strain, depleted of a repressor of nearby toxin genes (28), exhibited slow single-cell growth, as well as bulging, filamentation, and some explosive lysis (Fig. 3D). Length variability likely reflected differences in the timing of toxin induction. These findings suggest that a variety of single-cell phenotypes can be responsible for the variability in length caused by slight knockdown of essential genes.

The knockdown strain targeting the known modulator of cell width *mreB* (29) exhibited significant increases in width, as did strains targeting genes implicated in the maintenance of outer membrane integrity, such as *lolCDE*, *lspA*, *lpxB*, *kdsB*, and *lgt* (Fig. 3A). Indeed, knockdown strains targeting outer membrane function genes were significantly enriched among wide strains ($P < 5 \times 10^{-5}$, hypergeometric test). A previous study quantified the morphology of all nonessential gene deletions (21) and found that the deletion of genes involved in the synthesis of the enterobacterial common antigen (ECA) caused significant increases in cell width, potentially by sequestering the undecaprenyl phosphate lipid carrier also required by peptidoglycan synthesis (30, 31).

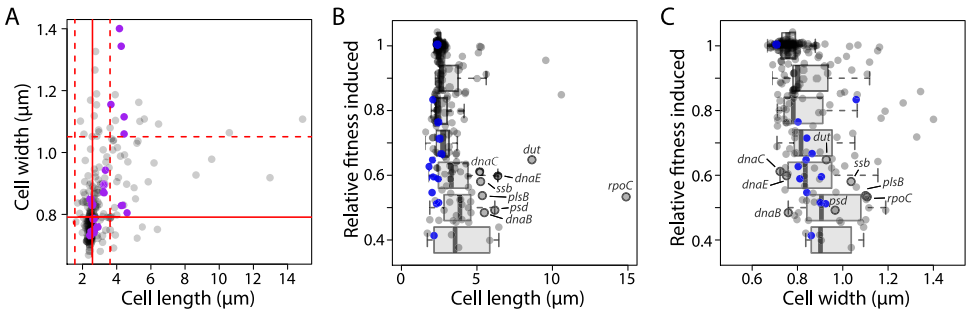

FIG 4 Fully induced CRISPRi targeting of essential genes results in morphological phenotypes characteristic of stress responses. (A) Median length and width for all strains after full induction of CRISPRi. Purple dots represent outer membrane-related genes. Solid red lines indicate the median width and length, and the red dashed lines indicate ±3 SD from the median, estimated from the median absolute distance. (B and C) Altered cell length and width were associated with reduced relative fitness, suggesting a connection between morphological defects and growth. Box plots show the distributions of median strain length and width within bins of 0.1 RF. tRNA synthases, represented by blue dots, exhibited short length (B) but normal width (C), consistent with the induction of the stringent response. Genes discussed in the text as exhibiting low relative fitness and filamentation are outlined by black circles.

Our finding that slight depletion of genes involved in lipoprotein trafficking (*lolCDE*) and modification (*lgt*), which do not involve an undecaprenyl phosphate lipid carrier, also cause a significant increase in cell width suggests that a different mechanism may be involved, perhaps related to the mechanical properties of the outer membrane (32) or to the depletion of lipoproteins involved in cell wall synthesis. In addition to genes with direct roles in shape determination, we also identified genes likely to have indirect effects on cell shape, including *ribA*, *pth*, *holB*, *panC*, and *ileS* (Table S3). Although operon effects are likely responsible for some of these phenotypes (e.g., *holB* is upstream of *mltG*, *ileS* is upstream of *lspA*), others are likely due to biologically meaningful indirect effects.

Terminal morphologies reveal novel modulators of stress pathways. Measurements of cellular morphology at a low level of CRISPRi activity (basal induction) revealed direct modulators of cell size. To determine how strong (fully induced) depletion of essential genes affects cellular physiology, we quantified the morphology of each strain after 5.5 h of growth in fresh LB with 1 mM IPTG. As expected, more strains exhibited strong cell dimension phenotypes (26%; 59/239) than in the absence of inducer (Fig. 4A). A total of 26 strains were significantly wider than the median (>3 SD wider than the median), and 47 strains were significantly longer (Table S3). Atypical dimensions were associated with decreased fitness (RF) in the pooled screen (Fig. 4B and C) and therefore may represent the indirect effects of stress responses pathways, such as the SOS response and the stringent response, which are activated by potentially lethal challenges such as strong depletion of essential genes (33, 34).

Filamentation due to cell division inhibition is canonically associated with the SOS response, a deeply conserved pathway that senses DNA damage and halts cell division until the damage can be repaired (35). Of the 29 strains that grew poorly ($RF_{induced} < 0.7$) and were significantly longer (>3 SD more than the median; Table S3), we focused on the 10 with the clearest filamentation phenotypes (median length $> 5\ \mu$m). Consistent with SOS induction causing filamentation, depletion of genes directly or indirectly involved in DNA replication, such as *dnaBCE*, *dut*, and *ssb*, was associated with strong filamentation phenotypes. However, not all strong filamentation resulted from SOS induction. For example, knockdown of *rpoC* caused the strongest filamentation phenotype in our screen (median length $> 14\ \mu$m) (Table S3). Inhibition of RpoC using a cyclopeptide inhibitor (36) was previously shown to cause SOS-independent filamentation (37). Depletion of the phospholipid synthesis genes *psd* and *plsB* also caused filamentation, consistent with previous studies (38), although whether these phenotypes manifest through the SOS response remains to be determined.

Strains also exhibited phenotypes consistent with activation of the stringent response. The stringent response is induced by uncharged tRNAs and prepares cells for starvation by downregulating translation, upregulating amino acid synthesis, and arresting the cell cycle (39). Activation of the stringent response is associated with decreased cell length (40–42). We identified 16 strains (Fig. 4B) with substantial growth rate decreases ($RF_{induced} < 0.7$) and decreased length (below the median of all strains) (Fig. 4B). Consistent with these phenotypes resulting from stringent response activation, 8 of these 16 strains target tRNA synthases and 2 target amino acid synthesis genes (*dapD* and *glyA*). In addition to these strains, strains targeting *adk*, *ribA*, *ribC*, *kdsA*, *yihA*, and *ppa* exhibited a similar phenotype. *adk*, which encodes adenosine kinase, was recently implicated as a potential activator of the stringent response (43). Depletion of genes involved in riboflavin synthesis (*ribA* and *ribC*) likely activates the stringent response through one or more of the 38 *E. coli* flavoenzymes, many of which are metabolic enzymes (44). No studies currently implicate genes involved in lipopolysaccharide (LPS) synthesis (*kdsA*), inorganic pyrophosphatase (*ppa*), or the cell cycle-related GTPase (*yihA*) as playing a role in the stringent response. It remains to be determined if the small-cell-size phenotypes observed for these strains are due to indirect activation of the stringent response or to other stress response pathways.

***mreB* is subject to negative transcriptional feedback.** Unlike other approaches for modulating essential gene expression, such as promoter replacement (45), CRISPRi modulation of gene expression is responsive to native transcriptional feedback circuits (14, 46). We focused our attention on the actin homolog *mreB*, which has no characterized transcriptional feedback (47, 48) but exhibits strikingly different susceptibility to knockdown in *B. subtilis* and *E. coli* (15). Whereas *mreB* knockdown in *B. subtilis* results in substantial lysis after 10 generations, similar *mreB* knockdown in *E. coli* does not substantially affect fitness (15). To determine if negative transcriptional feedback is responsible for the robustness of *E. coli* to *mreB* knockdown, we assayed the expression of *mreB*, as well as genes with (*rho*) (49) and without (*fabB/fabI*) known homeostatic feedback regulation in the presence of various degrees of CRISPRi knockdown using reverse transcription-quantitative PCR (RT-qPCR) (see Materials and Methods). As expected, both *fabB* and *fabI* exhibited monotonically decreasing knockdown as the CRISPRi system was induced (Fig. 5A). In contrast, *rho* and *mreB* expression levels were not affected by slight (uninduced) CRISPRi knockdown. Full induction of the CRISPRi system resulted in substantial downregulation of *rho* and *mreB* (Fig. 5A), suggesting that the sgRNAs targeting *rho* and *mreB* are functional, and that the lack of observed knockdown in the uninduced experiment is due to the activation of native feedback circuits, which can be overcome with sufficiently high levels of repression.

To determine if *mreB* is subject to transcriptional feedback, we constructed a fluorescent reporter in which the *mreB* promoter drives *gfp* expression from an upstream region containing the native promoter and the 5′ end of the gene (27) including the CRISPRi-targeted spacer (Fig. S5A) and performed time-lapse imaging of log-phase cells harboring this reporter (without CRISPRi induction). Slight *mreB* knockdown led to heterogeneous cell widths (Fig. 5B). We grouped cells by their width at time zero into two groups: those with wild type-like widths (cell width < 1.4 μm) and cells much wider than the wild type (cell width ≥ 1.4 μm). Wide cells exhibited lower *mreB* expression (Fig. 5C), which gradually increased during imaging, concurrent with a decrease in width (Fig. 5C and D). Because the *mreB* promoter contains three putative transcriptional start sites (TSSs) (50), we constructed two additional reporters, encompassing truncated versions of the promoter. All three fluorescent reporters behaved similarly (Fig. 5C; Fig. S5B and C). These data are consistent with a transcriptional feedback circuit regulating MreB expression and suggest that the first TSS is sufficient for feedback regulation.

To confirm that the observed increase in fluorescence was due to feedback, we constructed and measured a feedback reporter, which was identical to our full-length transcriptional reporter except that the protospacer-adjacent motif (PAM) targeted by the CRISPRi system was mutated (Fig. S5A). This reporter is therefore not affected by

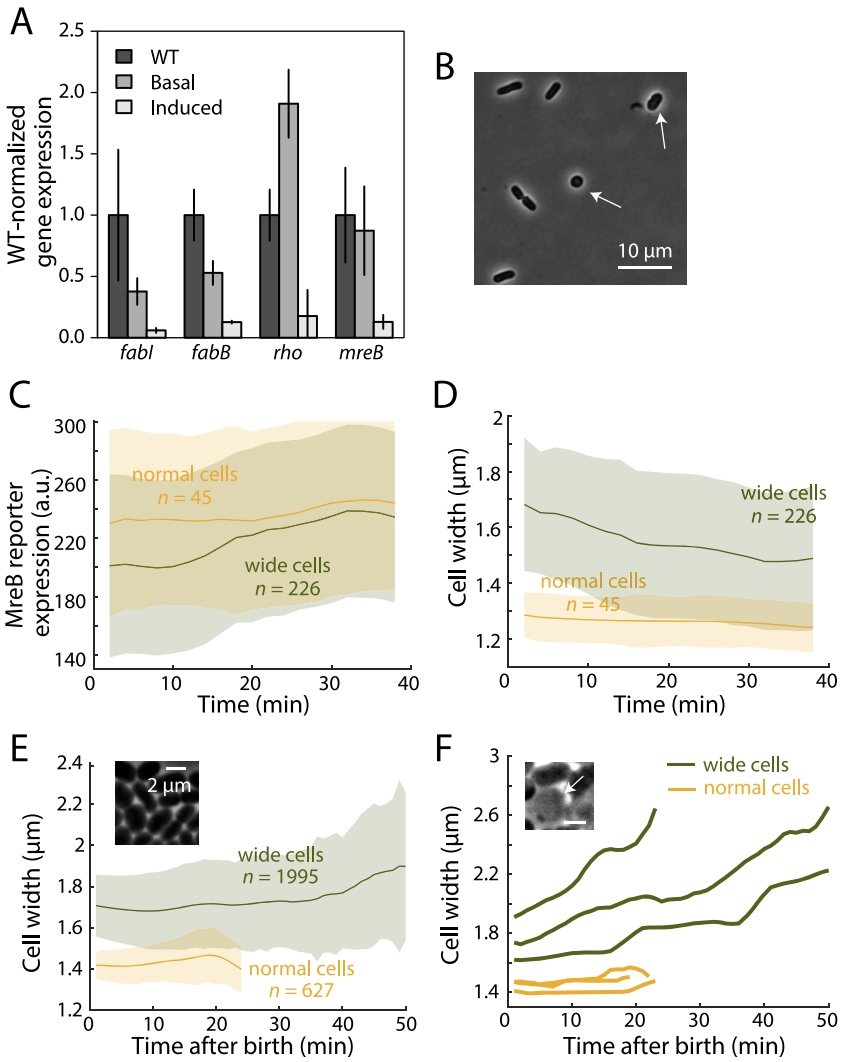

FIG 5 Transcriptional feedback on *mreB* expression is critical for width control and cell viability. (A) RT-qPCR measurements of the effect of basal and full CRISPRi induction on *fabI*, *fabB*, *rho*, and *mreB* expression normalized to the expression of those genes in the wild-type strain. Expression levels of *rho* and *mreB* were not inhibited by basal induction of CRISPRi but were decreased by the fully induced system. (B) Slight knockdown (no IPTG) of *mreB* led to shape heterogeneity in which some cells were substantially wider (white arrows). (C and D) Time-lapse imaging of the *mreB* knockdown strain with a TSS1 reporter. Wider cells exhibited lower MreB expression, but MreB expression increased in these cells during the imaging (C), concurrent with a decrease in cell width (D), demonstrating transcriptional-level feedback. (E) In a strain with *mreB* under the control of an inducible IPTG-regulated synthetic promoter (to eliminate transcriptional feedback), wide cells continued to increase in width when cultured in a microfluidic device with continuous flow of fresh nutrient. (Inset) Cells in the microfluidic device exhibited large variations in cell width. Data in panels C to E are means and SD. (F) Typical cell width traces for the experiment shown in panel E. While cells with normal width grew and divided normally, once cell width increased to $>$1.6 μm, they continued to increase in width, failed to divide, and eventually lysed. (Inset) A cell that lysed due to failure in width control.

CRISPRi, and hence, its expression reports only upregulation in response to perturbation of expression at the native locus. Wide cells exhibited higher expression of this reporter (Fig. S5D), confirming that *mreB* expression was responsive to cell width.

Finally, to determine if the putative feedback mechanism senses the level of *mreB* expression or the activity of the elongation system, we measured the expression of the full-length *mreB* reporter in the presence of A22 or amdinocillin. A22 causes cell widening by depolymerizing MreB filaments and inhibiting MreB activity but does not directly alter *mreB* expression (51). Amdinocillin targets PBP2, a component of the

essential cell wall synthase of the elongation machinery, which also leads to cell widening via its interactions with the cell wall synthesis machinery and MreB (51). Both A22 and amdinocillin treatment resulted in increased expression of the full-length *mreB* reporter concurrent with cell widening (Fig. S5E and F), suggesting that transcriptional regulation of the *mreB* promoter occurs in response to elongation system activity rather than *mreB* expression. The mechanistic details of this newly discovered response remain to be elucidated.

Transcriptional feedback is critical for cell shape maintenance and stability. We next sought to determine the importance of transcriptional feedback on *mreB* for cell width maintenance. To do so, we eliminated normal transcriptional controls by using a strain in which *mreB* (but not its promoter, which drives *mreCD* expression) is deleted from the chromosomal locus and provided on a plasmid under the control of an inducible IPTG-regulated synthetic promoter (52). In the presence of 10 μM or 100 μM IPTG, this strain did not exhibit growth defects during normal daily passaging. The width of this strain depended on external IPTG levels and was between that of the wild-type strain and that of the uninduced *mreB* CRISPRi strain (Fig. S5G), suggesting that IPTG-induced MreB expression was somewhat less than in the wild-type strain but more than in the *mreB* CRISPRi strain. However, when we attempted to propagate this strain in steady-state exponential growth in a microfluidic device with continuous flow of fresh medium and 100 μM IPTG, cells exhibited variations in cell width after several doublings (Fig. 5E, inset). Once these cells increased in width beyond $\sim$1.6 μm, they continued to widen, failed to divide, and eventually lysed (Fig. 5E and F). Similar dynamics were observed at lower IPTG concentrations, where cells lost width control more rapidly (Fig. S5H). In contrast, *mreB* CRISPRi knockdown cells wider than 1.6 μm were able to counteract continued widening and avoid lysis (Fig. 5D). Cell lysis and loss of width control were also observed in test tubes when the IPTG-inducible *mreB* strain underwent repeated dilutions to maintain an OD of $<$0.1, indicating that the observed phenotype is not specific to growth in microfluidic devices. These data suggest that transcriptional feedback at the native *mreBCD* locus is necessary for the stable maintenance of cell width and that disrupting this regulation leads to fluctuations that disrupt *E. coli* cell width, especially during extended periods of steady-state, exponential growth.

DISCUSSION

Here, we constructed an arrayed library of chromosomally encoded CRISPRi strains targeting the essential genes of the model bacterium *E. coli* and used it to study their functional importance. Our CRISPRi system, which was designed with a constitutively expressed *dcas9* and an inducible sgRNA for fast turn-on, is flexible and allows the use of different *dcas9* constructs. Although numerous CRISPRi studies have been performed in *E. coli* and other Gram-negative bacteria, to date all arrayed CRISPRi libraries have been constructed in Gram-positive species (12). Because many differences between Gram-positive and Gram-negative bacteria are found in essential structures such as the outer membrane and the divisome, our library will be a powerful resource for the microbiology community.

Previous work suggested that decreases in translational capacity could result in long lag times, but the essentiality of most ribosomal proteins meant that this hypothesis could not easily be tested (24). We showed that slight knockdown of essential ribosomal proteins is sufficient to substantially lengthen lag phase (Fig. 2), emphasizing the role of translational capacity during growth transitions and explaining a previous observation that ribosomal protein genes are upregulated very early in lag phase (53). Reduced translational capacity during lag phase led to a surprising phenotype: for several hours, cells grew with linear rather than exponential dynamics. This behavior was followed by a transition to exponential growth, which generally occurred $\sim$30 min before cell division (Fig. 2F). Determining how translational capacity is linked to cell

division during growth transitions will open exciting new windows into regulation of the bacterial cell cycle.

Profiling the cellular dimensions of our knockdown strains under slight (basal) and strong (fully induced) knockdown revealed previously unrecognized aspects of bacterial physiology. Under slight knockdown, most strains were able to grow at near-wild-type rates. As a result, we identified strains in which cell shape was directly impacted by knockdown, such as those targeting lipoprotein export genes (*lolCDE* and *lgt*), which exhibited high cell width potentially caused by changes to the mechanical properties of the outer membrane or by decreases in the levels of lipoproteins involved in cell wall synthesis. Fully inducing the CRISPRi system led to more extreme morphological defects, which were associated with decreased growth rates and presumably represented the action of cellular stress responses. For example, strong knockdown of genes involved in DNA synthesis (*dnaBCE*, *dut*, and *ssb*) led to filamentation, likely by activating the SOS response. Similarly, knockdown of many tRNA synthases led to short cells, likely due to activation of the stringent response. Further studies to determine which stress responses are induced in response to the depletion of specific essential processes will deepen our understanding of the myriad ways bacteria survive antibiotic and chemical challenges.

Previously, we found that *E. coli* could tolerate significant knockdown of the essential operon *mreBCD*, while *B. subtilis* could not (15). Our *E. coli* results were supported by a study that found limited knockdown when targeting *mreC* using a different CRISPRi system (54) and by the limited fitness effects of CRISPRi repression of the *Enterobacter cloacae mreCD* genes (55). We speculated that the robustness of the *mreBCD* operon to CRISPRi may be due to transcriptional feedback (15), which can mitigate or even overcome CRISPRi repression (14, 46). Using a series of fluorescent feedback and expression reporters, we found that transcriptional feedback was responsible for mitigating CRISPRi repression of *mreB*. Moreover, analysis of a strain in which *mreB* is placed under the control of a synthetic inducible promoter suggested that feedback control of the *mreBCD* locus is required for the stability of width control. In *E. coli*, the *mreBCD* operon is negatively regulated by BolA (47), which is conserved in Gram-negative but not Gram-positive bacteria (56). However, BolA appears unlikely to be responsible for the observed transcriptional feedback, because its deletion is viable and does not alter cell shape in exponential phase (21). Thus, our data suggest that a hitherto-undiscovered and critical regulatory mechanism is responsible for maintaining consistent MreB activity in the face of external perturbations.

Arrayed libraries of CRISPRi strains targeting essential genes have already demonstrated their usefulness in Gram-positive bacteria, greatly contributing to our understanding of essential gene function and the interplay between essential processes (8–11). We anticipate that the *E. coli* library described here will set the stage for similarly powerful advances in Gram-negative bacteria.

MATERIALS AND METHODS

Microbes. *Escherichia coli* strains were cultured in LB medium at 37°C. Antibiotics used were gentamicin (10 μg/ml), chloramphenicol (25 μg/ml), kanamycin (30 μg/ml), A22 (10 μg/ml), and amdinocillin (1 μg/ml).

CRISPRi library design. sgRNAs were designed to target genes in *E. coli* BW25113 for which there is some evidence of essentiality in published data sets, as summarized in Table S1. sgRNAs were designed to target within each gene's ORF near the 5′ end and bind the nontemplate strand, and sgRNAs with multiple potential binding sites were avoided, as previously described (8). sgRNA design scripts are publicly available at https://github.com/traeki/sgrna_design.

CRISPRi strain construction. The lambda att-integrating plasmid pCAH63 (19) was modified to contain an sgRNA expression cassette to generate pCs-550r in the following steps: the sgRNA constant region was cloned from pgRNA-bacteria (Addgene number 44251) (7); the terminators L3S3P22 and L3S2P21 were cloned up- and downstream, respectively, to flank the sgRNA cassette; and the sgRNA promoter was changed from BBa_J23119 to PlLac-O1 (57). New 20-nucleotide spacers were cloned into pCs-550r via inverse PCR (58), Sanger sequenced, and transformed into *E. coli* BW25113 harboring pINT-ts to promote integration at lambda att (19) using $CaCl_2$ competence and selecting for chloramphenicol resistance.

High-efficiency conjugation was used to transfer *dcas9* from the chromosome of a donor strain to the chromosome of a sgRNA-encoding recipient strain. A pseudo-Hfr strain isogenic to BW25113 carries

the transfer region from F and a spectinomycin marker integrated downstream of *rhaM* (59). The *dcas9* donor strain was constructed by integrating *dcas9* and a gentamicin resistance marker at the Tn*7* att site (60), adjacent to the origin of transfer, using the Mobile-CRISPRi triparental mating strategy (55). To clone the Tn*7* cassette plasmid, *dcas9* was amplified from pdCas9-bacteria (Addgene number 44249) under the control of the synthetic promoter BBa_J23105 (http://parts.igem.org/). Conjugation was performed on LB plates by mixing the *dcas9* donor and sgRNA recipient in equal ratios, incubating for 5 h at 37°C, pinning onto double-selection plates (chloramphenicol plus gentamicin), and growing overnight. Single colonies from each conjugation mix were isolated by streaking onto double-selection plates.

RFP strain construction. The *rfp* cassette including a Kan^r marker was PCR amplified from the entry vector used to construct the previously described red fluorescent protein (RFP) reporter strain (plasmid, pSLQ1232; strain, MG1655 *nfsA*::PlLac-O1-*mrfp*) (7). The *rfp* promoter was changed from PLlac-O1 to a minimal synthetic promoter (BBa_J23119; http://parts.igem.org/Main_Page) to create pSLQ1232-P541-rfp and then integrated into BW25113 at *nfsA* by λ*red* recombineering (61) and selecting for kanamycin resistance. Promoter variants were cloned along with *dcas9* into the Tn*7* cassette plasmid, and triparental mating was used to introduce *dcas9* cassette into the chromosome at Tn*7* att, as described above.

Flow cytometry to quantify knockdown and reporter activities. Flow cytometry analysis of the RFP reporter strains was performed as described in reference 62 with minor modifications; strains were initially inoculated from single colonies and grown for ~5 h before dilution instead of overnight. Data were collected on an LSRII flow cytometer (BD Biosciences) using the yellow/green laser (561 nm) and the phycoerythrin (PE)-Texas Red detector (610/20 nm). Data for at least 20,000 cells were collected, and median fluorescence values were extracted using FlowJo (FlowJo, LLC). Data from representative samples were plotted as histograms using FlowJo.

CRISPRi library construction. sgRNA plasmids were cloned, verified, and integrated into *E. coli* BW25113 as described for individual strains above. One isolate of each sgRNA recipient was stored by inoculating into 250 μl LB with chloramphenicol in deep 96-well plates, grown for 6.5 h, mixed with glycerol, and stored at −80°C. Arrayed sgRNA recipient libraries and the arrayed *dcas9* donor strain were pinned from glycerol stocks to separate LB agar plates using a ROTOR robot (Singer Instruments) and grown overnight. The arrayed recipient library was then mixed with the arrayed donor strain by pinning onto a new LB agar plate and then grown for 8 h to allow conjugation. Patches were mixed and transferred to a double-selection agar plate (gentamicin and chloramphenicol) using the ROTOR robot and grown overnight. Patches were each individually struck out on double-selection plates for single-colony isolation. To store the CRISPRi library, 2 isolates of each strain were inoculated in 250 μl LB with chloramphenicol and gentamicin supplemented with 0.2% glucose in deep 96-well plates, grown for 6.5 h, mixed with glycerol, and stored at −80°C in 96-well plates.

CRISPRi library sequencing. The sgRNA regions were first amplified from frozen stocks using round 1 forward and reverse primers (Table S1) and then cleaned up using an Exo-CIP PCR cleanup kit (NEB). The PCR products were diluted 1:50 and amplified again using custom primers containing Nextera adapters and indices. Samples were then pooled and cleaned using a NucleoSpin PCR cleanup kit (TaKaRa). Sequencing was performed on an Illumina NextSeq 500 system. Spacer sequences were extracted from fastq files and counted by exact matching to the designed library sequences.

Pooled library construction. To enable the use of deep sequencing to quantify relative fitness, an additional ~50 nontargeting sgRNA plasmids were cloned and integrated into BW25113, as described above. Control sgRNA spacers were selected as a random subset from previously characterized control sgRNAs (15). Construction of the pooled library (all library sgRNAs plus control sgRNAs) was identical to that of the arrayed library, except that after the second double selection of the arrayed library, all patches were scraped from the agar plate, thoroughly mixed, and stored as glycerol stocks at −80°C.

Pooled growth experiment. To quantify the relative fitness of each CRISPRi strain, we enumerated the relative proportion of each sgRNA spacer in the mixed population by deep sequencing, before and after 15 doublings in saturating IPTG. Briefly, a single glycerol stock of the pooled library was fully thawed, inoculated into 10 ml LB at an OD_{600} of 0.01, and grown for 2.5 h (final OD_{600} ~0.3). This culture was collected (10 ml, time [*t*] = 0) and used to inoculate replicate 4-ml LB cultures (with or without 1 mM IPTG) at an OD_{600} of 0.01, which were then repeatedly grown for 130 min to an OD_{600} of 0.3 (~5 doublings) and back-diluted to 0.01 a total of 3 times (to allow 15 doublings). After growth back to an OD_{600} of 0.3, cultures were collected (4 ml) by pelleting (9,000 × *g* for 2 min) and stored at −80°C. The following day, genomic DNA was extracted using the DNeasy blood and tissue kit (Qiagen number 69506) with the recommended Gram-negative pretreatment and RNase A treatment. sgRNA spacer sequences were amplified from gDNA using Q5 polymerase (New England Biolabs number M0493S) for 14 cycles using custom primers containing TruSeq adapters and indices, followed by gel purification from 8% Tris-borate-EDTA (TBE) gels.

Spacer sequences were extracted from fastq files, counted by exact matching to expected library spacers, and their counts were normalized within each sample to control for read depth. We calculated the fitness as relative fitness (15), wherein the $\log_2$ fold change was normalized by the median $\log_2$ fold change of the control sgRNAs and adjusted by the number of doublings. All RF values are reported in Table S2.

Population-level growth analyses. To measure growth dynamics, overnight cultures were inoculated into 80 μl of fresh medium in a clear 384-well plate. The plate was covered with an optical film, with small holes poked at the side of each well to allow aeration. Incubation and OD measurements were performed with an Epoch 2 plate reader (BioTek) at 37°C with continuous shaking, and OD_{600} was measured at 8.5-min intervals. The instantaneous growth rates were calculated as the slope of ln(OD) with respect to time after smoothing using a moving average filter with a window size of 5. Maximum

growth rate was calculated as the largest instantaneous growth rate. Lag time was defined as the duration before cells reaching half of their maximum growth rate.

To normalize per-strain growth rates and lag times due to inoculation effects, a 384-well plate containing only wild-type cells was grown and analyzed as described above. The maximum growth rate and lag time of each CRISPRi strain was compared to the median for the 10 wild-type replicates with the closest starting optical density.

Morphological analyses. Overnight cultures were inoculated into fresh medium and grown to log phase in multiwell plates. For microscopy images with a single time point, the MATLAB (MathWorks, Natick, MA, USA) image processing code Morphometrics (63) was used to segment cells and to identify cell outlines from phase-contrast or fluorescence microscopy images. For time-lapse imaging, raw images were first segmented with the machine learning algorithm DeepCell (64) and then processed with Morphometrics to obtain cell contours. A local coordinate system was generated for each cell outline using a meshing method adapted from MicrobeTracker (65). Cell widths were calculated by averaging the distances between contour points perpendicular to the cell midline, excluding contour points within the poles and sites of septation. Cell length was calculated as the length of the midline from pole to pole. The meshing method failed on cells that lose rod shape. Therefore, for the *mreB* data in Fig. 5E and F and Fig. S5H, length and width were defined as the dimensions of the major and minor principal axes of the cell contour.

For each strain, average cellular dimensions were estimated by first eliminating all cells with widths of <0.6 μm or >2.0 μm (except for the *mreB* data in Fig. 5 and Fig. S5, where no width filtering was performed) and then, if at least 100 cells remained, calculating the median cell length and width. Coefficients of variation (CV) were estimated using the median absolute distance multiplied by 1.4826 to robustly estimate the standard deviation.

To correct for plate effects caused by imaging uninduced cells in 96-well plates rather than in 384-well plates, each of the seven 96-well plates was normalized by subtracting the median length and width of all strains on the plate from the values of each strain and then adding back the global median length and width.

Single-cell time-lapse imaging. Overnight cultures were diluted 1:100 and placed onto 1% agarose pads containing LB. For imaging experiments with log-phase cells, overnight cultures were diluted 1:200 into a test tube and grown for 2 h prior to imaging. Phase-contrast images and epifluorescence images (for reporter strains) were acquired with a Nikon Ti-E inverted microscope (Nikon Instruments) using a 100X (numerical aperture [NA], 1.40) oil immersion objective and a Neo 5.5 sCMOS camera (Andor Technology). The microscope was outfitted with an active-control environmental chamber for temperature regulation (HaisonTech, Taipei, Taiwan). Images were acquired using μManager v.1.4 (66).

Microfluidics. Overnight cultures were diluted 1:200 and incubated at 37°C for 2 h with shaking. Cells were then loaded into B04A microfluidic perfusion plates (CellASIC). Imaging was performed with a constant flow of fresh LB medium with IPTG at 2 lb/in^2.

Transcriptional reporter plasmid construction and quantification. We used transcriptional reporter plasmids selected from, or designed to mimic, a previously described library of reporter plasmids (27). If the desired reporter was not a member of the library, the upstream region (150 to 400 bp upstream of the ORF and 50 to 100 bp within the ORF and containing the targeted protospacer) was amplified by PCR (Table S1) from BW25113 genomic DNA with 25 bp of flanking sequence and assembled by HiFi (New England Biolabs number E2621L) with the PCR-amplified pUA66 vector. In the case of feedback reporters, PAM mutations were introduced by quick-change mutagenesis (Table S1). Plasmids were transformed into CRISPRi strains by electroporation, selecting for kanamycin resistance. GFP fluorescence was quantified by summing the intensity values of each pixel within the cell contour after subtracting background fluorescence and normalized to the projected area of the cell.

RT-qPCR experiment design and analysis. *E. coli* CRISPRi strains were grown in triplicate from single colonies in prewarmed 4 ml LB for 2.5 h before back-dilution (1:80) in prewarmed 4 ml LB with or without 1 mM IPTG and growth for 3 h prior to collection (OD_{600} ~0.2). The control strains express *rfp* with or without an sgRNA targeting *rfp* ("nontargeting") and were treated identically. Samples were collected (300 μl) in 900 μl TRIzol-LS (Thermo Fisher number 10296010) and stored at −20°C overnight. The following day, RNA was extracted according to the TRIzol protocol. RNA was quantified using a NanoDrop 2000c spectrophotometer (Thermo Scientific) to normalize input (500 ng input per 20-μl reaction). For each RT-qPCR probe set and each sample replicate, reactions were performed in triplicate. All RT-qPCR assays were performed using the Luna Universal one-step RT-qPCR kit (New England Biolabs number E3005S) according to its RT and cycling protocols in 96-well PCR plates (Neptune number 3732.X) and measured on a CFX Connect real-time system (Bio-Rad).

Standard curves for each primer pair were first assessed on serially diluted RNA extracted from the CRISPRi control strain to confirm single melting peaks and strong correlations of technical replicates and to calculate their efficiencies in accordance with reference 67. Measured primer efficiencies were used to calculate the relative expression of each gene of interest in each experimental sample relative to the reference gene (*recA*).

Statistical methods. Unless otherwise described, robust statistics were used. The mean was estimated using the median, the standard deviation was estimated by multiplying the median absolute distance by 1.4826, and all linear regressions were performed using MM-estimation as implemented in the robustbase R package.

Strain availability. The sgRNA library, which has been single colony purified and sequence verified, will be available for distribution through the Coli Genetic Stock Center (CGSC). Mating these strains with

the pseudo-Hfr *dcas9* strain (also available from CGSC) or otherwise introducing dCas9 (e.g., on a plasmid) will allow researchers to quickly generate a CRISPRi strain of interest.

Data availability. All data referenced are available in the supplemental materials. All raw sequencing data used to calculate relative fitness have been deposited in the Short Read Archive under accession number PRJNA669343. All raw sequencing data used to determine strain purity have been deposited in the Short Read Archive under accession number PRJNA728203.

SUPPLEMENTAL MATERIAL

Supplemental material is available online only.

FIG S1, PDF file, 0.1 MB.

FIG S2, PDF file, 1.1 MB.

FIG S3, PDF file, 1.3 MB.

FIG S4, PDF file, 0.9 MB.

FIG S5, PDF file, 0.5 MB.

TABLE S1, XLSX file, 0.4 MB.

TABLE S2, XLSX file, 0.1 MB.

TABLE S3, XLSX file, 0.1 MB.

ACKNOWLEDGMENTS

We thank members of the K.C.H. and C.A.G. laboratories for extensive helpful discussions, J. Garabino for help with flow cytometry, R. Shields for sharing *Streptococcus mutans* growth data, and E. Chow, D. Bogdanoff, and K. Chaung from the UCSF Center for Advanced Technology for help with sequencing. We thank B. M. Koo for his heroic effort in preparing sequencing libraries for all sgRNA and CRISPRi strains.

M.R.S. was supported by the National Institutes of Health T32 GM007810a training grant and a National Science Foundation Graduate Research Fellowship. H.S. was supported by an Agilent Graduate Fellowship, a Stanford Interdisciplinary Graduate Fellowship, and a James S. McDonnell Postdoctoral Fellowship. This work was supported in part by the National Institutes of Health grants F32 GM108222 and K22AI137122 (to J.M.P.), F32AI133917 (to M.R.), RM1 GM135102 (to K.C.H.), and R35 GM118061 (to C.A.G.), the Innovative Genomics Institute, UC Berkeley (to C.A.G.), National Science Foundation Career Award MCB-1149328 (to K.C.H.), and the Allen Discovery Center at Stanford on Systems Modeling of Infection (to K.C.H.). K.C.H. is a Chan Zuckerberg Biohub Investigator.

We have no conflicts of interest to declare.

REFERENCES

1. Baba T, Ara T, Hasegawa M, Takai Y, Okumura Y, Baba M, Datsenko KA, Tomita M, Wanner BL, Mori H. 2006. Construction of *Escherichia coli* K-12 in-frame, single-gene knockout mutants: the Keio collection. Mol Syst Biol 2:2006.0008. https://doi.org/10.1038/msb4100050.
2. Nichols RJ, Sen S, Choo YJ, Beltrao P, Zietek M, Chaba R, Lee S, Kazmierczak KM, Lee KJ, Wong A, Shales M, Lovett S, Winkler ME, Krogan NJ, Typas A, Gross CA. 2011. Phenotypic landscape of a bacterial cell. Cell 144:143–156. https://doi.org/10.1016/j.cell.2010.11.052.
3. Koo B-M, Kritikos G, Farelli JD, Todor H, Tong K, Kimsey H, Wapinski I, Galardini M, Cabal A, Peters JM, Hachmann A-B, Rudner DZ, Allen KN, Typas A, Gross CA. 2017. Construction and analysis of two genome-scale deletion libraries for *Bacillus subtilis*. Cell Syst 4:291–305.E7. https://doi.org/10.1016/j.cels.2016.12.013.
4. Price MN, Wetmore KM, Jordan Waters R, Callaghan M, Ray J, Liu H, Kuehl JV, Melnyk RA, Lamson JS, Suh Y, Carlson HK, Esquivel Z, Sadeeshkumar H, Chakraborty R, Zane GM, Rubin BE, Wall JD, Visel A, Bristow J, Blow MJ, Arkin AP, Deutschbauer AM. 2018. Mutant phenotypes for thousands of bacterial genes of unknown function. Nature 557:503–509. https://doi.org/10.1038/s41586-018-0124-0.
5. Lalanne J-B, Taggart JC, Guo MS, Herzel L, Schieler A, Li G-W. 2018. Evolutionary convergence of pathway-specific enzyme expression stoichiometry. Cell 173:749–761.E38. https://doi.org/10.1016/j.cell.2018.03.007.
6. Bikard D, Jiang W, Samai P, Hochschild A, Zhang F, Marraffini LA. 2013. Programmable repression and activation of bacterial gene expression using an engineered CRISPR-Cas system. Nucleic Acids Res 41:7429–7437. https://doi.org/10.1093/nar/gkt520.
7. Qi LS, Larson MH, Gilbert LA, Doudna JA, Weissman JS, Arkin AP, Lim WA. 2013. Repurposing CRISPR as an RNA-guided platform for sequence-specific control of gene expression. Cell 152:1173–1183. https://doi.org/10.1016/j.cell.2013.02.022.
8. Peters JM, Colavin A, Shi H, Czarny TL, Larson MH, Wong S, Hawkins JS, Lu CHS, Koo B-M, Marta E, Shiver AL, Whitehead EH, Weissman JS, Brown ED, Qi LS, Huang KC, Gross CA. 2016. A comprehensive, CRISPR-based functional analysis of essential genes in bacteria. Cell 165:1493–1506. https://doi.org/10.1016/j.cell.2016.05.003.
9. Liu X, Gallay C, Kjos M, Domenech A, Slager J, van Kessel SP, Knoops K, Sorg RA, Zhang J-R, Veening J-W. 2017. High-throughput CRISPRi phenotyping identifies new essential genes in *Streptococcus pneumoniae*. Mol Syst Biol 13:931. https://doi.org/10.15252/msb.20167449.
10. Shields RC, Walker AR, Maricic N, Chakraborty B, Underhill SAM, Burne RA. 2020. Repurposing the *Streptococcus mutans* CRISPR-Cas9 system to understand essential gene function. PLoS Pathog 16:e1008344. https://doi.org/10.1371/journal.ppat.1008344.
11. de Wet TJ, Winkler KR, Mhlanga M, Mizrahi V, Warner DF. 2020. Arrayed CRISPRi and quantitative imaging describe the morphotypic landscape of essential mycobacterial genes. Elife 9:e60083. https://doi.org/10.7554/eLife.60083.

12. Todor H, Silvis MR, Osadnik H, Gross CA. 2021. Bacterial CRISPR screens for gene function. Curr Opin Microbiol 59:102–109. https://doi.org/10.1016/j.mib.2020.11.005.
13. Wang T, Guan C, Guo J, Liu B, Wu Y, Xie Z, Zhang C, Xing X-H. 2018. Pooled CRISPR interference screening enables genome-scale functional genomics study in bacteria with superior performance. Nat Commun 9:2475. https://doi.org/10.1038/s41467-018-04899-x.
14. Rousset F, Cui L, Siouve E, Becavin C, Depardieu F, Bikard D. 2018. Genome-wide CRISPR-dCas9 screens in *E. coli* identify essential genes and phage host factors. PLoS Genet 14:e1007749. https://doi.org/10.1371/journal.pgen.1007749.
15. Hawkins JS, Silvis MR, Koo B-M, Peters JM, Osadnik H, Jost M, Hearne CC, Weissman JS, Todor H, Gross CA. 2020. Mismatch-CRISPRi reveals the co-varying expression-fitness relationships of essential genes in *Escherichia coli* and *Bacillus subtilis*. Cell Syst 11:523–535.E9. https://doi.org/10.1016/j.cels.2020.09.009.
16. Rishi HS, Toro E, Liu H, Wang X, Qi LS, Arkin AP. 2020. Systematic genome-wide querying of coding and non-coding functional elements in *E. coli* using CRISPRi. bioRxiv https://doi.org/10.1101/2020.03.04.975888.
17. Mutalik VK, Adler BA, Rishi HS, Piya D, Zhong C, Koskella B, Kutter EM, Calendar R, Novichkov PS, Price MN, Deutschbauer AM, Arkin AP. 2020. High-throughput mapping of the phage resistance landscape in *E. coli*. PLoS Biol 18:e3000877. https://doi.org/10.1371/journal.pbio.3000877.
18. Mathis AD, Otto RM, Reynolds KA. 2021. A simplified strategy for titrating gene expression reveals new relationships between genotype, environment, and bacterial growth. Nucleic Acids Res 49:e6. https://doi.org/10.1093/nar/gkaa1073.
19. Haldimann A, Wanner BL. 2001. Conditional-replication, integration, excision, and retrieval plasmid-host systems for gene structure-function studies of bacteria. J Bacteriol 183:6384–6393. https://doi.org/10.1128/JB.183.21.6384-6393.2001.
20. Donati S, Kuntz M, Pahl V, Farke N, Beuter D, Glatter T, Gomes-Filho JV, Randau L, Wang C-Y, Link H. 2021. Multi-omics analysis of CRISPRi-knockdowns identifies mechanisms that buffer decreases of enzymes in *E. coli* metabolism. Cell Syst 12:56–67.E6. https://doi.org/10.1016/j.cels.2020.10.011.
21. Campos M, Govers SK, Irnov I, Dobihal GS, Cornet F, Jacobs-Wagner C. 2018. Genomewide phenotypic analysis of growth, cell morphogenesis, and cell cycle events in *Escherichia coli*. Mol Syst Biol 14:e7573. https://doi.org/10.15252/msb.20177573.
22. Cui L, Vigouroux A, Rousset F, Varet H, Khanna V, Bikard D. 2018. A CRISPRi screen in *E. coli* reveals sequence-specific toxicity of dCas9. Nat Commun 9:1912. https://doi.org/10.1038/s41467-018-04209-5.
23. Calvo-Villamañán A, Ng JW, Planel R, Ménager H, Chen A, Cui L, Bikard D. 2020. On-target activity predictions enable improved CRISPR-dCas9 screens in bacteria. Nucleic Acids Res 48:e64. https://doi.org/10.1093/nar/gkaa294.
24. Takeuchi R, Tamura T, Nakayashiki T, Tanaka Y, Muto A, Wanner BL, Mori H. 2014. Colony-live—a high-throughput method for measuring microbial colony growth kinetics—reveals diverse growth effects of gene knockouts in *Escherichia coli*. BMC Microbiol 14:171. https://doi.org/10.1186/1471-2180-14-171.
25. Peters JM, Silvis MR, Zhao D, Hawkins JS, Gross CA, Qi LS. 2015. Bacterial CRISPR: accomplishments and prospects. Curr Opin Microbiol 27:121–126. https://doi.org/10.1016/j.mib.2015.08.007.
26. Monds RD, Lee TK, Colavin A, Ursell T, Quan S, Cooper TF, Huang KC. 2014. Systematic perturbation of cytoskeletal function reveals a linear scaling relationship between cell geometry and fitness. Cell Rep 9:1528–1537. https://doi.org/10.1016/j.celrep.2014.10.040.
27. Zaslaver A, Bren A, Ronen M, Itzkovitz S, Kikoin I, Shavit S, Liebermeister W, Surette MG, Alon U. 2006. A comprehensive library of fluorescent transcriptional reporters for *Escherichia coli*. Nat Methods 3:623–628. https://doi.org/10.1038/nmeth895.
28. Krishnamurthi R, Ghosh S, Khedkar S, Seshasayee ASN. 2017. Repression of YdaS toxin is mediated by transcriptional repressor RacR in the cryptic rac prophage of *Escherichia coli* K-12. mSphere 2:e00392-17. https://doi.org/10.1128/mSphere.00392-17.
29. Shi H, Bratton BP, Gitai Z, Huang KC. 2018. How to build a bacterial cell: MreB as the foreman of *E. coli* construction. Cell 172:1294–1305. https://doi.org/10.1016/j.cell.2018.02.050.
30. Jorgenson MA, Kannan S, Laubacher ME, Young KD. 2016. Dead-end intermediates in the enterobacterial common antigen pathway induce morphological defects in *Escherichia coli* by competing for undecaprenyl phosphate. Mol Microbiol 100:1–14. https://doi.org/10.1111/mmi.13284.
31. Jorgenson MA, Young KD. 2016. Interrupting biosynthesis of O antigen or the lipopolysaccharide core produces morphological defects in *Escherichia coli* by sequestering undecaprenyl phosphate. J Bacteriol 198:3070–3079. https://doi.org/10.1128/JB.00550-16.
32. Rojas ER, Billings G, Odermatt PD, Auer GK, Zhu L, Miguel A, Chang F, Weibel DB, Theriot JA, Huang KC. 2018. The outer membrane is an essential load-bearing element in Gram-negative bacteria. Nature 559:617–621. https://doi.org/10.1038/s41586-018-0344-3.
33. Poole K. 2012. Bacterial stress responses as determinants of antimicrobial resistance. J Antimicrob Chemother 67:2069–2089. https://doi.org/10.1093/jac/dks196.
34. Lai GC, Cho H, Bernhardt TG. 2017. The mecillinam resistome reveals a role for peptidoglycan endopeptidases in stimulating cell wall synthesis in *Escherichia coli*. PLoS Genet 13:e1006934. https://doi.org/10.1371/journal.pgen.1006934.
35. Baharoglu Z, Mazel D. 2014. SOS, the formidable strategy of bacteria against aggressions. FEMS Microbiol Rev 38:1126–1145. https://doi.org/10.1111/1574-6976.12077.
36. Delgado MA, Rintoul MR, Farías RN, Salomón RA. 2001. *Escherichia coli* RNA polymerase is the target of the cyclopeptide antibiotic microcin J25. J Bacteriol 183:4543–4550. https://doi.org/10.1128/JB.183.15.4543-4550.2001.
37. Salomón RA, Farías RN. 1992. Microcin 25, a novel antimicrobial peptide produced by *Escherichia coli*. J Bacteriol 174:7428–7435. https://doi.org/10.1128/jb.174.22.7428-7435.1992.
38. Hawrot E, Kennedy EP. 1978. Phospholipid composition and membrane function in phosphatidylserine decarboxylase mutants of *Escherichia coli*. J Biol Chem 253:8213–8220. https://doi.org/10.1016/S0021-9258(17)34384-3.
39. Irving SE, Choudhury NR, Corrigan RM. 2021. The stringent response and physiological roles of (pp)pGpp in bacteria. Nat Rev Microbiol 19:256–271. https://doi.org/10.1038/s41579-020-00470-y.
40. Schreiber G, Ron EZ, Glaser G. 1995. ppGpp-mediated regulation of DNA replication and cell division in *Escherichia coli*. Curr Microbiol 30:27–32. https://doi.org/10.1007/BF00294520.
41. Büke F, Grilli J, Lagomarsino MC, Bokinsky G, Tans S. 2020. ppGpp is a bacterial cell size regulator. bioRxiv https://doi.org/10.1101/2020.06.16.154187.
42. Ferullo DJ, Lovett ST. 2008. The stringent response and cell cycle arrest in *Escherichia coli*. PLoS Genet 4:e1000300. https://doi.org/10.1371/journal.pgen.1000300.
43. Roghanian M, Semsey S, Løbner-Olesen A, Jalalvand F. 2019. (p)ppGpp-mediated stress response induced by defects in outer membrane biogenesis and ATP production promotes survival in *Escherichia coli*. Sci Rep 9:2934. https://doi.org/10.1038/s41598-019-39371-3.
44. Langer S, Hashimoto M, Hobl B, Mathes T, Mack M. 2013. Flavoproteins are potential targets for the antibiotic roseoflavin in *Escherichia coli*. J Bacteriol 195:4037–4045. https://doi.org/10.1128/JB.00646-13.
45. Keren L, Hausser J, Lotan-Pompan M, Vainberg Slutskin I, Alisar H, Kaminski S, Weinberger A, Alon U, Milo R, Segal E. 2016. Massively parallel interrogation of the effects of gene expression levels on fitness. Cell 166:1282–1294.E18. https://doi.org/10.1016/j.cell.2016.07.024.
46. Vigouroux A, Oldewurtel E, Cui L, Bikard D, van Teeffelen S. 2018. Tuning dCas9's ability to block transcription enables robust, noiseless knockdown of bacterial genes. Mol Syst Biol 14:e7899. https://doi.org/10.15252/msb.20177899.
47. Freire P, Moreira RN, Arraiano CM. 2009. BolA inhibits cell elongation and regulates MreB expression levels. J Mol Biol 385:1345–1351. https://doi.org/10.1016/j.jmb.2008.12.026.
48. Cayrol B, Fortas E, Martret C, Cech G, Kloska A, Caulet S, Barbet M, Trépout S, Marco S, Taghbalout A, Busi F, Wegrzyn G, Arluison V. 2015. Riboregulation of the bacterial actin-homolog MreB by DsrA small noncoding RNA. Integr Biol (Camb) 7:128–141. https://doi.org/10.1039/c4ib00102h.
49. Matsumoto Y, Shigesada K, Hirano M, Imai M. 1986. Autogenous regulation of the gene for transcription termination factor *rho* in *Escherichia coli*: localization and function of its attenuators. J Bacteriol 166:945–958. https://doi.org/10.1128/jb.166.3.945-958.1986.
50. Wachi M, Osaka K, Kohama T, Sasaki K, Ohtsu I, Iwai N, Takada A, Nagai K. 2006. Transcriptional analysis of the *Escherichia coli mreBCD* genes responsible for morphogenesis and chromosome segregation. Biosci Biotechnol Biochem 70:2712–2719. https://doi.org/10.1271/bbb.60315.
51. van Teeffelen S, Wang S, Furchtgott L, Huang KC, Wingreen NS, Shaevitz JW, Gitai Z. 2011. The bacterial actin MreB rotates, and rotation depends on cell-wall assembly. Proc Natl Acad Sci U S A 108:15822–15827. https://doi.org/10.1073/pnas.1108999108.

52. Shi H, Colavin A, Bigos M, Tropini C, Monds RD, Huang KC. 2017. Deep phenotypic mapping of bacterial cytoskeletal mutants reveals physiological robustness to cell size. Curr Biol 27:3419–3429.E4. https://doi.org/10.1016/j.cub.2017.09.065.
53. Rolfe MD, Rice CJ, Lucchini S, Pin C, Thompson A, Cameron ADS, Alston M, Stringer MF, Betts RP, Baranyi J, Peck MW, Hinton JCD. 2012. Lag phase is a distinct growth phase that prepares bacteria for exponential growth and involves transient metal accumulation. J Bacteriol 194:686–701. https://doi.org/10.1128/JB.06112-11.
54. Reis AC, Halper SM, Vezeau GE, Cetnar DP, Hossain A, Clauer PR, Salis HM. 2019. Simultaneous repression of multiple bacterial genes using nonrepetitive extra-long sgRNA arrays. Nat Biotechnol 37:1294–1301. https://doi.org/10.1038/s41587-019-0286-9.
55. Peters JM, Koo B-M, Patino R, Heussler GE, Hearne CC, Qu J, Inclan YF, Hawkins JS, Lu CHS, Silvis MR, Harden MM, Osadnik H, Peters JE, Engel JN, Dutton RJ, Grossman AD, Gross CA, Rosenberg OS. 2019. Enabling genetic analysis of diverse bacteria with Mobile-CRISPRi. Nat Microbiol 4:244–250. https://doi.org/10.1038/s41564-018-0327-z.
56. Huynen MA, Spronk CAEM, Gabaldón T, Snel B. 2005. Combining data from genomes, Y2H and 3D structure indicates that BolA is a reductase interacting with a glutaredoxin. FEBS Lett 579:591–596. https://doi.org/10.1016/j.febslet.2004.11.111.
57. Lutz R, Bujard H. 1997. Independent and tight regulation of transcriptional units in *Escherichia coli* via the LacR/O, the TetR/O and AraC/I1-I2 regulatory elements. Nucleic Acids Res 25:1203–1210. https://doi.org/10.1093/nar/25.6.1203.
58. Larson MH, Gilbert LA, Wang X, Lim WA, Weissman JS, Qi LS. 2013. CRISPR interference (CRISPRi) for sequence-specific control of gene expression. Nat Protoc 8:2180–2196. https://doi.org/10.1038/nprot.2013.132.
59. Typas A, Nichols RJ, Siegele DA, Shales M, Collins SR, Lim B, Braberg H, Yamamoto N, Takeuchi R, Wanner BL, Mori H, Weissman JS, Krogan NJ, Gross CA. 2008. High-throughput, quantitative analyses of genetic interactions in *E. coli*. Nat Methods 5:781–787. https://doi.org/10.1038/nmeth.1240.
60. Choi K-H, Schweizer HP. 2006. mini-Tn7 insertion in bacteria with single attTn7 sites: example *Pseudomonas aeruginosa*. Nat Protoc 1:153–161. https://doi.org/10.1038/nprot.2006.24.
61. Thomason LC, Sawitzke JA, Li X, Costantino N, Court DL. 2014. Recombineering: genetic engineering in bacteria using homologous recombination. Curr Protoc Mol Biol 106:1.16.1–16.1.39.
62. Rauch BJ, Silvis MR, Hultquist JF, Waters CS, McGregor MJ, Krogan NJ, Bondy-Denomy J. 2017. Inhibition of CRISPR-Cas9 with bacteriophage proteins. Cell 168:150–158.E10. https://doi.org/10.1016/j.cell.2016.12.009.
63. Ursell T, Lee TK, Shiomi D, Shi H, Tropini C, Monds RD, Colavin A, Billings G, Bhaya-Grossman I, Broxton M, Huang BE, Niki H, Huang KC. 2017. Rapid, precise quantification of bacterial cellular dimensions across a genomic-scale knockout library. BMC Biol 15:17. https://doi.org/10.1186/s12915-017-0348-8.
64. Van Valen DA, Kudo T, Lane KM, Macklin DN, Quach NT, DeFelice MM, Maayan I, Tanouchi Y, Ashley EA, Covert MW. 2016. Deep learning automates the quantitative analysis of individual cells in live-cell imaging experiments. PLoS Comput Biol 12:e1005177. https://doi.org/10.1371/journal.pcbi.1005177.
65. Sliusarenko O, Heinritz J, Emonet T, Jacobs-Wagner C. 2011. High-throughput, subpixel precision analysis of bacterial morphogenesis and intracellular spatio-temporal dynamics. Mol Microbiol 80:612–627. https://doi.org/10.1111/j.1365-2958.2011.07579.x.
66. Edelstein AD, Tsuchida MA, Amodaj N, Pinkard H, Vale RD, Stuurman N. 2014. Advanced methods of microscope control using μManager software. J Biol Methods 1:e10. https://doi.org/10.14440/jbm.2014.36.
67. Bustin SA, Benes V, Garson JA, Hellemans J, Huggett J, Kubista M, Mueller R, Nolan T, Pfaffl MW, Shipley GL, Vandesompele J, Wittwer CT. 2009. The MIQE guidelines: minimum information for publication of quantitative real-time PCR experiments. Clin Chem 55:611–622. https://doi.org/10.1373/clinchem.2008.112797.
68. Rousset F, Cabezas-Caballero J, Piastra-Facon F, Fernández-Rodríguez J, Clermont O, Denamur E, Rocha EPC, Bikard D. 2021. The impact of genetic diversity on gene essentiality within the *Escherichia coli* species. Nat Microbiol 6:301–312. https://doi.org/10.1038/s41564-020-00839-y.